RSC Advances

PAPER

View Article Online
View Journal | View Issue

Cite this: *RSC Adv.*, 2020, **10**, 27706

Fast, efficient and clean adsorption of bisphenol-A using renewable mesoporous silica nanoparticles from sugarcane waste ash†

Suzimara Rovani, *[a] Jonnatan J. Santos,[b] Sabine N. Guilhen,[a] Paola Corio[b] and Denise A. Fungaro[a]

Even with all the biological problems associated with bisphenol-A (BPA), this chemical is still being widely used, especially in thermal paper receipts. In this study, renewable mesoporous silica nanoparticles (MSN), obtained from sugarcane ash, functionalized with hexadecyltrimethylammonium (CTAB) were applied as an adsorbent in the removal of BPA from the aqueous solution. The versatility of this material and its BPA adsorption capacity were tested at different pH values, being practically constant at pH between 4 and 9, with a slight increase in pH 10 and a greater increase in pH 11. The removal time evaluation indicates a very fast adsorption process, removing almost 90% of BPA in the first 20 min of contact. The kinetic model indicates a monolayer formation of BPA molecules on the MSN-CTAB surface. The maximum adsorption capacity (Q_{max}) was 155.78 mg g^{-1}, one of the highest found in literature, and the highest for material from a renewable source.

Received 12th June 2020
Accepted 13th July 2020

DOI: 10.1039/d0ra05198e

rsc.li/rsc-advances

1. Introduction

Bisphenol-A (BPA) is an endocrine disruptive compound (EDC) that may mimic or interfere with the endocrine or hormonal system.[1] BPA was first synthesized in 1891 by Dianin[2] but its synthesis was first reported only in 1905 by Zincke.[3] BPA was widely used in the manufacture of thermal paper,[4] food storage containers, baby bottles, reusable drink containers, toys, dish and laundry detergents, bar soaps, shampoo, shaving cream, face cleansers, sunscreen lotions, *etc.*[5] Some effects of BPA on health are sexual dysfunction and fertility; metabolic disease, such as, obesity; cancer (breast cancer, neuroblastoma); neurological effects (disruption of the dopaminergic system); cardiovascular diseases; thyroid disorders and asthma.[1,6] BPA can also alter plasma sex hormones levels in fishes[7] and cause adverse effects in the development and reproduction of the non-mammalian aquatic vertebrates, including reduced male hormones, testicular cell death, decreased sperm density and motility, inhibition of spermatogenesis and egg production.[8]

Nowadays most plastic containers and personal care products are produced without BPA. However, aquatic bodies are still contaminated with bisphenol-A. The EDC can arrive in river waters from discharging industrial waste, in groundwater by leaching dump sites (mainly leaching from BPA-based plastics or microplastics)[9] and in tap water because conventional wastewater treatment processes are not completely efficient.[10,11] However, the biggest concern is that even though the problems caused by BPA it is still widely used, especially in thermal paper receipts.[4,12]

Many researchers have investigated the BPA removal by adsorption using different adsorbents, such as clays,[13,14] zeolites,[15,16] chitosan,[17,18] and agricultural wastes.[19,20]

A decade ago, Dong *et al.* 2010 (ref. 21) prepared zeolite from coal fly ash with low and high CaO content. In order to improve the adsorption of organic pollutants, the researchers modified the zeolites with the surfactant hexadecyltrimethylammonium (CTAB). The sample with a high Ca content reached the highest capacity for the removal of bisphenol-A. Later, Zhang *et al.* 2017 (ref. 22) synthesized SiO_2 from tetraethyl orthosilicate by a sol–gel method, modified it with CTAB and applied to adsorb BPA. The prepared adsorbent had a core/shell structure (core = CTAB micelle) and (shell = SiO_2). The results of this study indicated that the CTAB-core of the adsorbent had a dominant role in increasing the BPA removal capacity.

Considering these known properties of adsorbents modified with CTAB, in 2018, we reported for the first time, the synthesis of silica nanoparticles from sugarcane waste ash modified with CTAB. In that publication, we did a complete characterization of the material. The material's morphology was demonstrated by electron and transmission microscopy, the surface area was provided by BET method, pore size and shape were obtained by

[a]*Instituto de Pesquisas Energéticas e Nucleares, IPEN-CNEN/SP, Av. Prof. Lineu Prestes, 2242 Cidade Universitária, São Paulo, SP, CEP 05508-000, Brazil. E-mail: suzirovani@gmail.com*

[b]*Instituto de Química, Universidade de São Paulo, Av. Prof. Lineu Prestes, 748 Cidade Universitária, São Paulo, SP, CEP 05508-000, Brazil*

† Electronic supplementary information (ESI) available: Kinetic and equilibrium equations, UV spectra before and after BPA adsorption, BPA analytical curve at pH 11, additional TG curves, kinetic and isotherm parameters of BPA adsorption on MSN-CTAB. See DOI: 10.1039/d0ra05198e

N_2 adsorption–desorption isotherm, pore distribution by BJH method and the amount of CTAB on the silica particles was given by thermogravimetric analyses.[23] In this article, we go further with these renewable mesoporous silica nanoparticles, applying them to the adsorption/removal of BPA in aqueous solution. The effects of the various adsorption parameters, such as solution pH, contact time, and initial concentration of the BPA solution were studied and optimized.

2. Experimental

2.1. Materials

All aqueous solutions were prepared using deionized water (resistivity > 18.2 MΩ cm) obtained from a MilliQ deionizer (Elix Millipore). Sodium hydroxide micropearls (>99%), hydrochloric acid (35–37%), and *n*-butyl alcohol (>99%) were purchased from Synth, Brazil. Sulfuric acid (95–97%) and CTAB (≥98%) were purchased from Merck, Germany. Bisphenol-A was purchased from Sigma-Aldrich, United States of America. Sugarcane waste ash was donated by COSAN S. A., Brazil.

2.2. Methods

2.2.1. Preparation of mesoporous silica nanoparticles functionalized with hexadecyltrimethylammonium (MSN-CTAB). The renewable adsorbent material, mesoporous silica nanoparticles functionalized with hexadecyltrimethylammonium (MSN-CTAB) was prepared according to Rovani *et al.* 2018.[23]

Briefly, in a round bottom flask, CTAB (2%, w:w) was dissolved in a mixture of water and butyl alcohol (1 : 1, v/v) and heated to 60 °C. To this biphasic system, the sodium silicate solution (concentration 5.42%, w:w) obtained from sugarcane waste ash (as previously reported[23–25]) was added, under constant agitation. Then, a solution of sulfuric acid (0.5 mol L^{-1}) was added to this solution, drop by drop, until the pH decreased to 4, and the resulting gel was aged at 60 °C for 8 h. The gel of silica nanoparticles aged was washed with distilled water, filtered and oven dried at 120 °C.[23]

2.2.2. Bisphenol-A (BPA) adsorption study. The adsorption studies of bisphenol-A (BPA) onto MSN-CTAB were conducted at different pH values and initial BPA concentration of 100 mg L^{-1}. The experiments were carried out agitating the BPA solution with MSN-CTAB at 190 rpm using an adsorbent dosage of 1.0 g L^{-1} at different contact times, varying from 0 to 180 min. All experiments were performed in triplicate and at room temperature. The concentration of BPA before and after adsorption was detected by an UV-visible spectrophotometer (Varian, Cary 1E, USA). To measure the absorbance of samples after BPA adsorption, they were centrifuged at 1560*g*, the supernatant was removed, and then, their absorbance was measured.[23]

The amount of BPA removal was expressed as the removal percentage of contaminants and calculated by the eqn (1).

$$\%\ \text{removal} = \frac{(C_i - C_f)}{C_i} \times 100 \quad (1)$$

where C_i and C_f are the initial and final concentration of contaminants, respectively. The amount of contaminants adsorption as a function of time and at equilibrium, q_t and q_e (mg g^{-1}), respectively, were calculated using the following eqn (2):

$$q_t \text{ or } q_e = \frac{(C_i - C_e)}{m} \times V \quad (2)$$

where C_i, C_f and C_e (mg L^{-1}) are concentrations of contaminants at initial, final and equilibrium, respectively, V (L) is the volume of contaminants solution and m (g) is the mass of the adsorbent.[26,27]

The adsorption kinetics of BPA by MSN-CTAB, were tested using pseudo-first order[28,29] and pseudo-second order[30–32] models.[33–35] The Langmuir,[36] Freundlich[37] and Liu models were applied to fit the equilibrium data.[35] See the equations in ESI.†

2.3. Characterization

UV-vis spectra of samples, before and after BPA adsorption, were obtained using a Varian spectrophotometer, model Cary 1E (USA), utilizing quartz cuvettes with 10.0 mm path length, and scanning samples from 200 to 400 nm.

Fourier-transform infrared (FTIR) spectroscopy was performed using a spectrometer from Bruker, model Alpha (Germany), operating in attenuated total reflectance (ATR) mode. The spectra of samples were obtained using 200 cumulative scans, in the range of 375 to 4000 cm^{-1}.[23]

Thermogravimetric analyses were recorded in a thermogravimetric analyser TGA/SDTA from Mettler Toledo. Then, ~10.0 mg was weighed and analysed under an oxygen atmosphere with a flow of 50.0 mL min^{-1}, using an alumina-port sample heated to 900 °C with a heating rate of 10 °C min.[23,25] To obtain FTIR-ATR spectra and TG curves of MSN-CTAB after an interaction with BPA, the MSN-CTAB were isolated by centrifugation, dried for 5 h at 100 °C, and analysed.[23]

3. Results and discussion

The relative high solubility of this molecule or monomer, if analysed its application in the production of polymers, in water for an organic compound is a major concern (120–300 mg L^{-1} (21.5 °C)), especially from the hormonal point of view, as already mentioned.[10,11,38] In aqueous media with higher alkalinity, the solubility of BPA tends to increase, due to the dissociation of hydroxyl groups in its structure (Fig. 1).

The elimination of BPA using adsorbents creates the need to use an adsorbent capable of maintaining its properties at different pH values, without losing its adsorptive capacity. Fig. 2 shows a study of the effect of pH on BPA adsorption by MSN-CTAB.

As previously described,[23] the renewable adsorbent (MSN-CTAB) used in this study is composed of nanoparticles with

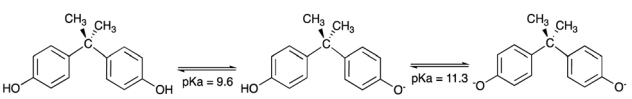

Fig. 1 Aqueous dissociation scheme of BPA with pK_a values.

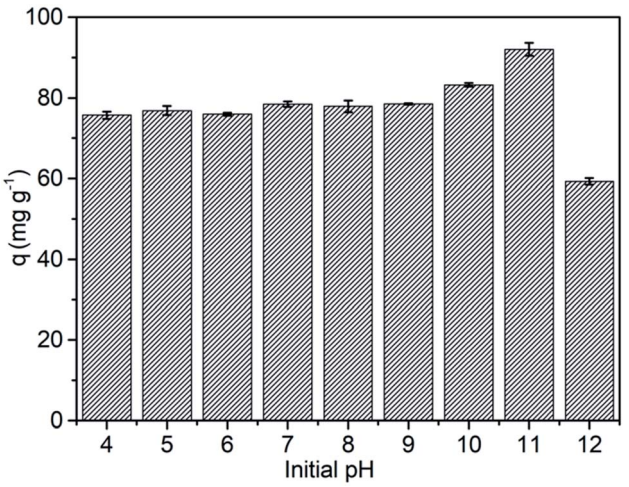

Fig. 2 Effect of the initial pH on the adsorption capacity of BPA. Conditions: 25 °C, initial concentration 100 mg L^{-1}, contact time 2 h and adsorbent mass 1.0 g L^{-1} (see Fig. S2 and Table S1†).

a size around 20 nm (Fig. S1†), specific surface area 131 m^2 g^{-1} (measured by BET), pore diameter of 22 nm (mesoporous materials) and CTAB composition estimated in 30%.[23] The results in Fig. 2 shows that the MSN-CTAB adsorption capacity for BPA adsorption was practically constant at pH values from 4 to 9 (75.74 to 78.54 mg g^{-1}), with a significant increase in adsorption capacity (83.28 mg g^{-1}) at pH 10 and the highest adsorption capacity (91.98 mg g^{-1}) at pH 11 (see Table S1†). On the other hand, at pH values higher than 12, a decrease in the adsorbent adsorption capacity was observed, this occurs because the silica nanoparticles dissolve in alkaline media where the pH is higher than 12.[39]

Interestingly, the increase in the adsorption capacity of MSN-CTAB coincided with the increase in BPA solubility, making its use attractive regardless of the pH of the medium.

Therefore, when the pH value of the BPA solution is below its pK_a values the BPA adsorption on MSN-CTAB occurs basically by hydrophobic interaction. And when the pH value of the BPA solution is between 9.6 to 11.3 the BPA adsorption on MSN-CTAB occurs also by electrostatic interaction, because MSN-CTAB has a higher affinity for anions when compared to the undissociated form of BPA.[22] At pH 11, BPA is mostly in the form of a bivalent anion. In this condition, it's likely that two CTAB molecules interact with one BPA molecule.

According to the literature, the interaction of the BPA anion occurs with the CTAB surfactant positively charged "head" in the inner layer, with the two BPA benzene rings pointing to the interior of the CTAB bilayers. When interacting with each surfactant layer, the two BPA benzene rings point into the CTAB hydrophobic phase, as this orientation allows the hydrophobic interaction between the BPA benzene ring and the CTAB 16-carbon tail, thus enhancing and thus enhances BPA adsorption,[21] as illustrated in Fig. 3.

Trying to exploit the maximum capacity of the adsorbent, a more complete study of bisphenol-A adsorption by MSN-CTAB

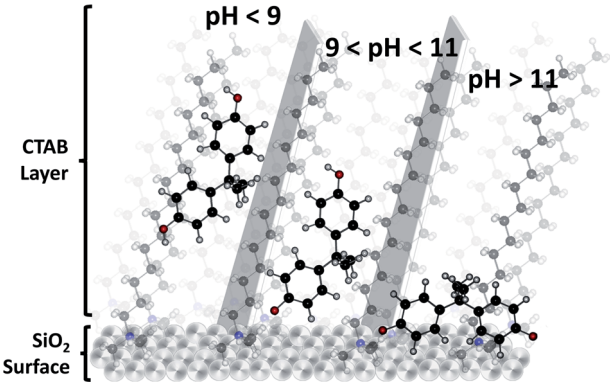

Fig. 3 Scheme illustrating the organization of BPA on the surface of MSN-CTAB at different pH values.

was performed at pH 11. The BPA calibration curve at pH 11 is shown in Fig. S3 (ESI).†

The adsorption kinetics study can provide multiple information about the adsorption velocity, the mechanism involving the adsorbent binding and the adsorption capacity of the material.

The rate of adsorption generally depends on the physicochemical characteristics of the adsorbate, adsorbent and solution, in which case the surfactant (used to mediate synthesis and modify silica nanoparticles) plays an important role. This surfactant has a positive charge. Kinetic results of BPA adsorption at 25 °C, at a contact time ranging from 0 to 180 min, for an initial concentration of 80.9 mg L^{-1} are shown in Fig. 4.

Analysing the experimental results, it is possible to notice that the adsorption process occurs very quickly in the first 20 minutes (reaching 89% of BPA adsorption), almost reaching saturation in 1 h (see Fig. S4b and Table S2†).

Considering that the process was carried out in batch, it is evident that BPA has a great affinity for this material (MSN-CTAB), since the adsorbent–adsorbate contact is not induced and occurs naturally.

This process could be improved by preparing membranes or columns for solid-state separation with MSN-CTAB and

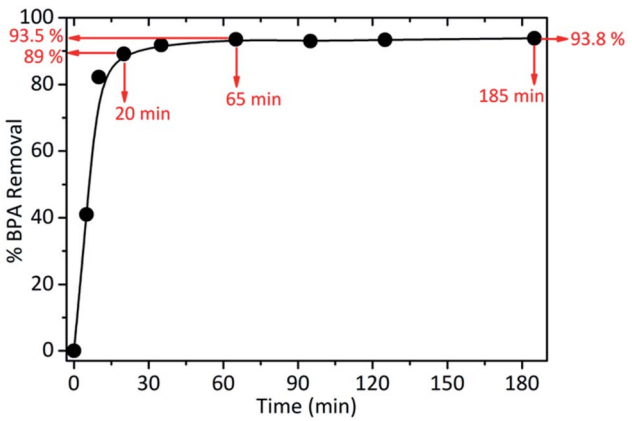

Fig. 4 Percentage of BPA removal at 25 °C, at a contact time ranging from 0 to 180 min (initial concentration of 80.9 mg L^{-1}).

allowing the solution to pass through this material. The kinetic results were fit using pseudo first[28] and pseudo second[30] order models[35] (see the equations in ESI†). The solid samples obtained after adsorption (MSN-CTAB + BPA), were analysed *via* FTIR and TGA, as can be seen in Fig. 5.

Considering the tested kinetic models, it is possible to observe a better fit for the pseudo-first-order model due to the higher $R_{adj.}^2$ value (0.9784), and lower chi-square (X^2) value (0.000519), Fig. 5a and Table S3.† Elovich and fractional power models[40] were also tested (Fig. S5 and Table S4†), however, the pseudo-first-order model remains the model that best fits the experimental data. The main reason that the fit of the curve, even for pseudo-first-order, is not perfect is in the adsorption kinetics, which seems to be very fast and the method used to measure the adsorption speed (UV-vis spectroscopy) very simple, which can generate some error. The calculated q_e value of the pseudo-first-order model was close to that found experimentally (Table S3†).

Kinetic models are important to describe the mechanism associated with the adsorption process of the analyte in the adsorbent, and are not associated with the system stoichiometry. In this case, this process may be related to the process of monolayer formation of BPA molecules on the MSN-CTAB surface.

In order to investigate the chemical composition of the MSN-CTAB, bisphenol-A and BPA adsorbed on the adsorbent, measurements were performed by FTIR spectroscopy. ATR mode infrared spectra of these samples are shown in Fig. 5b. The MSN-CTAB adsorbent has six major bands. The presence of CTAB in the silica structure is observed from the symmetrical and asymmetrical CH_2 stretching bands at 2850 and 2922 cm^{-1}, respectively. The bands at 799, 446 cm^{-1} are related to symmetrical stretching of the siloxane group, the strong band at 1058 cm^{-1} is attributed to the asymmetrical stretching of siloxane group and finally the band at 965 cm^{-1} is related to angular deformation –OH of silanol.[25]

The "blue" spectrum in Fig. 5b is from BPA adsorbed on the MSN-CTAB adsorbent, the bands at 568 and 554 cm^{-1} are mainly due to C–O and C–C. The band at 834 cm^{-1} is attributed to the =C–H out of plane deformation vibration, sets replacement pattern. The band at 1512 cm^{-1} is the result of the H–C–H interaction. Finally, the bands at 1592 and 1614 cm^{-1} are related to the absorption of aromatic compounds, C=C aromatic stretch vibrations. Harmonic bands at 1592 and 1614 cm^{-1} define ring replacement pattern.[41] The changes in the MSN-CTAB infrared spectra after the adsorption of BPA ("blue" spectrum in Fig. 5b) are in agreement with previous findings in the literature,[21] which suggested that the interaction mechanism between BPA and CTAB involved the phenolic

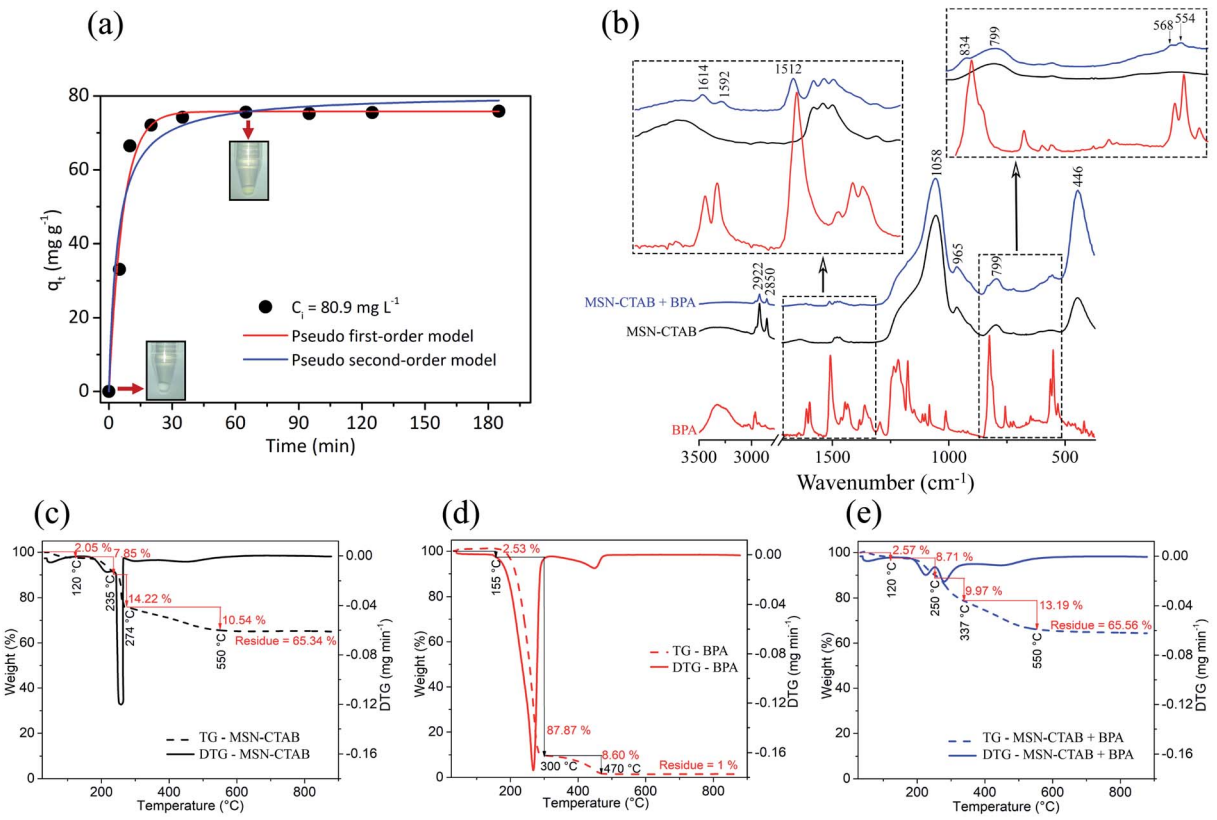

Fig. 5 (a) Pseudo first and second-order models kinetics plot for the removal of BPA by MSN-CTAB. Conditions: 25 °C, initial concentration 80.9 mg L^{-1} and adsorbent mass 1.0 g L^{-1} (more details in Table S3†). (b) FTIR-ATR spectra of bisphenol-A, MSN-CTAB and MSN-CTAB + bisphenol-A. And TG and DTG curves of (c) MSN-CTAB, (d) BPA and (e) MSN-CTAB + BPA. The measures were performed under an oxygen atmosphere (more details in Fig. S6 and Table S5†).

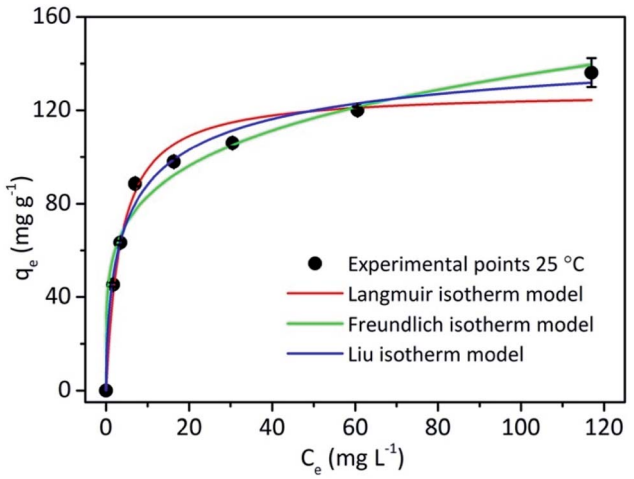

Fig. 6 Adsorption Langmuir and Freundlich isotherms for BPA adsorbed by silica nanoparticles. Conditions: 25 °C, contact time 1 h and adsorbent mass 1.0 g L^{-1} (see Fig. S7, Table S6 and S7†).

hydroxyl groups and the positively charged quaternary ammonium (see Fig. 3). The adsorption of BPA over MSN-CTAB (in pH 11) was mainly due to electrostatic interactions between the BPA negatively charged (–O$^-$) and the cationic micelle of the adsorbent.[22]

Fig. 5c–e shows only the TG curves of studied samples. The TG curve of MSN-CTAB (Fig. 5c) shows a first weight loss until 120 °C (2.05%) due to humidity loss, a second loss between 120 and 235 °C (7.85%) attributed to CTAB decomposition unbound on the MSN-CTAB (hydrophobic–hydrophobic interactions of interconnected CTAB). Still in Fig. 5c a third loss between 235 and 274 °C (14.22%) is related to the CTAB decomposition bound on the MSN-CTAB by electrostatic interaction.[23,42] Finally the fourth loss between 274 and 550 °C (10.54%) is attributed to complete decomposition of organic material on the surface of MSN-CTAB, leaving 65.34% of residue, that is, silica.

The TG curve of BPA (Fig. 5d) shows mass loss of almost 100%, which is characteristic of organic material. While the TG curves of the MSN-CTAB adsorbent (Fig. 5c) and of the BPA adsorbed on the adsorbent (Fig. 5e) present about 65% of residue, characteristic of the presence of inorganic material "silica". On the other hand, a small difference (between 300 and 550 °C) was observed for these two TG curves (see Fig. S6†), which is due to the loss of BPA adsorbed on the MSN-CTAB.[23]

TG curve of the BPA adsorbed on the MSN-CTAB (Fig. 5e) shows a difference of weight loss (second and third loss with displacement to higher temperatures) when compared to Fig. 5c and d, this effect also is related to the loss of BPA bound on the MSN-CTAB (see Table S5†).[23]

Adsorption isotherms, in turn, describe the relationship between the amount of adsorbate adsorbed by the adsorbent (q_e) and the concentration of adsorbate remaining in the solution after the system reaches equilibrium (C_e) at a constant temperature. In this study, Langmuir,[36] Freundlich[37] and Liu models were applied to fit the equilibrium data.[35] See the equations in ESI.† The Langmuir, Freundlich and Liu isotherm models are presented in Fig. 6.

Although the Langmuir model is an excellent model applied to processes involving the formation of particle/film surface monolayers of molecules at a finite and defined number of adsorption sites, the Freundlich model has a better application for non-homogeneous processes over heterogeneous surfaces, and is not limited to monolayer or any uniform distribution. Finally, the Liu model can be applied to a system that has characteristics of both systems mentioned above.[35]

Based on the isotherm parameters of Table S7,† the Liu model presented the best adjusted determination coefficient value ($R_{ajd.}^2$). The Q_{max} found in Liu's model was 155.78 mg g^{-1}, confirming that this is the best model for explaining the equilibrium of BPA adsorption by MSN-CTAB. In the model proposed by Liu, the active adsorbent sites do not have the same energy, which makes the adsorbent a preferred site for adsorption, leading to saturation.[35]

According to the literature, there are studies that report adsorbents more and others less efficient than the adsorbent studied here. Table 1 shows a comparison of the BPA adsorption capacities of different adsorbents of the literature.

Table 1 Comparison of BPA adsorption capacities of various adsorbents[a]

Adsorbent abbreviation	BET (m^2 g^{-1})	Soln pH	Time (h)	Q_{max} (mg g^{-1})	References
MSN-CTAB	131	11.0	1	155.78	This study
SMZFA F (zeolite)	91.5	10.4	24	114.9	Dong *et al.* 2010 (ref. 21)
SMZFA L (zeolite)	50.6	9.6	24	56.8	Dong *et al.* 2010 (ref. 21)
Y-type zeolite	504	7.0	< 2	111.1	Tsai *et al.* 2006 (ref. 15)
Vinyl-SiO_2 nanospheres	—	—	2	136.97	Zhou *et al.* 2013 (ref. 43)
MCM-41	1030	6–7	6	9.0	Kim *et al.* 2011 (ref. 44)
MMIPs (polymer)	—	6.0	0.5	106.38	Wang *et al.* 2016 (ref. 45)
CTAB–SiO_2	—	—	6	198.8	Zhang *et al.* 2017 (ref. 22)
Ph-MS (mesoporous)	750	6–7	6	351.0	Kim *et al.* 2011 (ref. 44)
PAC (powder AC)	1780	6–7	6	337.0	Kim *et al.* 2011 (ref. 44)
Activated carbon	1350	—	24	56.5	Asada *et al.* 2004 (ref. 46)
Porous carbon	300	—	24	41.8	Asada *et al.* 2004 (ref. 46)

[a] All adsorption experiments were carried out at room temperature.

According to Table 1 the adsorbent (MSN-CTAB from sugarcane waste ash) used in this study showed a higher maximum adsorption capacity when compared to zeolites/CTAB prepared with coal fly ash (SMZFA F and L),[21] in addition to shorter contact time in the adsorption process. MSN-CTAB also showed a higher BPA adsorption capacity than the adsorbents: hydrophobic Y-type zeolite;[15] vinyl-SiO_2 nanospheres;[43] MCM-41;[44] MMIPs[45] and activated carbon.[46]

We reached a Q_{max} value close to that found by Zhang *et al.* 2017,[22] for a similar adsorbent, with the difference that we used a renewable source to produce silica while Zhang *et al.* 2017,[22] used tetraethyl orthosilicate. Our adsorbent (MSN-CTAB) even with Q_{max} value of 155.78 mg g^{-1}, about 2 times smaller than adsorbents Ph-MS and PAC.[44] When converted to mg of BPA adsorbed per m^2 of surface area of the adsorbent, the MSN-CTAB (1.19 mg m^{-2}) has a higher value, when compared to Ph-MS[44] (0.468 mg m^{-2}) and PAC[44] (0.189 mg m^{-2}), what shows a higher affinity or better environment for adsorption of BPA.

4. Conclusions

In this study an adsorbent, MSN-CTAB, prepared from sugarcane waste ash, was used for BPA adsorption. Kinetic and isotherm models were tested, a better fit for the kinetic model was pseudo-first-order, in this case, this process may be related to the process of monolayer formation of BPA molecules on the MSN-CTAB surface. Liu isotherm model predicts the experimental data with Q_{max} = 155.78 mg g^{-1} and the adsorption equilibrium time was 60 min. The Liu model approached the Langmuir model (monolayer adsorption). Adsorption capacity of BPA by the adsorbent was practically constant at pH values between 4 and 9, there was a slight increase at pH 10 and a greater increase at pH 11. This was due to the fact that at pH 11 the BPA is mainly in the form of bivalent anion, and thus two CTAB molecules can interact with one BPA molecule. The BPA adsorption on MSN-CTAB occurred majority by hydrophobic interaction in pH values between 4 and 9 and by hydrophobic and electrostatic interaction at pH value above 10. According to the results obtained, the MSN-CTAB presents potential to be employed as adsorbent for remediation of water contaminated with endocrine disrupting compounds, such as, bisphenol-A.

Conflicts of interest

There are no conflicts to declare.

Acknowledgements

The authors acknowledge the COSAN/RAIZEN for supplying the sugarcane waste ash, the Dra. Nilce Ortiz who made the UV-vis spectrophotometer to collect UV-vis spectra available, and also the Dra. Duclerc F. Parra for TG analyses. This research was funded by Coordenação de Aperfeiçoamento de Pessoal de Nível Superior-Brasil (CAPES) – Código financeiro 001. We are also thankful to Conselho Nacional de Desenvolvimento Científico e Tecnológico-Brazil (CNPq) and Fundação de Amparo à Pesquisa do Estado de São Paulo-Brazil (FAPESP).

References

1 A. R. Brown, J. M. Green, J. Moreman, L. M. Gunnarsson, S. Mourabit, J. Ball, M. J. Winter, M. Trznadel, A. Correia, C. Hacker, A. Perry, M. E. Wood, M. J. Hetheridge, R. A. Currie and C. R. Tyler, *Environ. Sci. Technol.*, 2019, **53**, 463–474.
2 A. P. Dianin, *J. Russ. Phys.-Chem. Soc.*, 1891, **23**(523–546), 601–611.
3 T. Zincke, *Justus Liebigs Ann. Chem.*, 1905, **343**, 75–99.
4 D. M. Goldinger, A.-L. Demierre, O. Zoller, H. Rupp, H. Reinhard, R. Magnin, T. W. Becker and M. Bourqui-Pittet, *Regul. Toxicol. Pharmacol.*, 2015, **71**, 453–462.
5 A. Bhatnagar and I. Anastopoulos, *Chemosphere*, 2017, **168**, 885–902.
6 F. Maqbool, S. Mostafalou, H. Bahadar and M. Abdollahi, *Life Sci*, 2016, **145**, 265–273.
7 K. Ji, S. Hong, Y. Kho and K. Choi, *Environ. Sci. Technol.*, 2013, **47**, 8793–8800.
8 L. Canesi and E. Fabbri, *Dose Response*, 2015, **13**, 1559325815598304.
9 W. Wei, Q.-S. Huang, J. Sun, J.-Y. Wang, S.-L. Wu and B.-J. Ni, *Environ. Sci. Technol.*, 2019, **53**, 2509–2517.
10 S. Y. Wee and A. Z. Aris, *npj Clean Water*, 2019, **2**, 1–14.
11 J. Im and F. E. Löffler, *Environ. Sci. Technol.*, 2016, **50**, 8403–8416.
12 M. Eckardt, M. Kubicova, D. Tong and T. J. Simat, *J. Chromatogr. A*, 2020, **1609**, 11.
13 S. Zheng, Z. Sun, Y. Park, G. A. Ayoko and R. L. Frost, *Chem. Eng. J.*, 2013, **234**, 416–422.
14 S. I. Rathnayake, Y. Xi, R. L. Frost and G. A. Ayoko, *J. Colloid Interface Sci.*, 2016, **470**, 183–195.
15 W.-T. Tsai, H.-C. Hsu, T.-Y. Su, K.-Y. Lin and C.-M. Lin, *J. Colloid. Interface Sci.*, 2006, **299**, 513–519.
16 J. Li, Y. Zhan, J. Lin, A. Jiang and W. Xi, *Environ. Earth Sci.*, 2014, **72**, 3969–3980.
17 Y. Kimura, M. Yamamoto, R. Shimazaki, A. Kashiwada, K. Matsuda and K. Yamada, *J. Appl. Polym. Sci.*, 2012, **124**, 796–804.
18 M. H. Dehghani, M. Ghadermazi, A. Bhatnagar, P. Sadighara, G. Jahed-Khaniki, B. Heibati and G. McKay, *J. Environ. Chem. Eng.*, 2016, **4**, 2647–2655.
19 D. Balarak, *Int. J. Chemtech Res.*, 2016, **9**, 681–690.
20 B. Orimolade, F. Adekola, M. Aminat, A. Idris, O. Saliu and T. Yusuf, *J. Appl. Chem. Res.*, 2018, **12**, 8–21.
21 Y. Dong, D. Wu, X. Chen and Y. Lin, *J. Colloid Interface Sci.*, 2010, **348**, 585–590.
22 Y. Zhang, C. Liu, L. Luo, Y. Shi, Y. Chen, S. Wang, L. Bian and F. Jiang, *Water Sci. Technol.*, 2017, **76**, 928–938.
23 S. Rovani, J. J. Santos, P. Corio and D. A. Fungaro, *ACS Omega*, 2018, **3**, 2618–2627.
24 R. H. Alves, T. V. S. Reis, S. Rovani and D. A. Fungaro, *J. Chem.*, 2017, **2017**, 9.
25 S. Rovani, J. J. Santos, P. Corio and D. A. Fungaro, *J. Braz. Chem. Soc.*, 2019, **30**, 1524–1533.

26 S. Rovani, A. G. Rodrigues, L. F. Medeiros, R. Cataluña, É. C. Lima and A. N. Fernandes, *J. Environ. Chem. Eng.*, 2016, **4**, 2128–2137.
27 S. Neusatz Guilhen, S. Rovani, L. Pitol Filho and D. Alves Fungaro, *Chem. Eng. Commun.*, 2019, **206**, 1354–1366.
28 S. Lagergren, *K. Sven. Vetenskapsakad. Handl.*, 1898, **24**, 1–39.
29 Y. S. Ho and G. McKay, *Chem. Eng. J.*, 1998, **70**, 115–124.
30 G. Blanchard, M. Maunaye and G. Martin, *Water Res*, 1984, **18**, 1501–1507.
31 Y.-S. Ho, PhD thesis, University of Birmingham, 1995.
32 Y. S. Ho, D. A. J. Wase and C. F. Forster, *Environ. Technol.*, 1996, **17**, 71–77.
33 Y.-S. Ho, *J. Hazard. Mater.*, 2006, **136**, 681–689.
34 Y.-S. Ho, *Environ. Sci. Pollut. Res.*, 2014, **21**, 7234–7235.
35 É. C. Lima, M. A. Adebayo and F. M. Machado, in *Carbon Nanomaterials as Adsorbents for Environmental and Biological Applications*, ed. C. P. Bergmann and F. M. Machado, Springer International Publishing, 1st edn, 2015, ch. 3, pp. 33–69, DOI: 10.1007/978-3-319-18875-1.
36 I. Langmuir, *J. Am. Chem. Soc.*, 1918, **40**, 1361–1403.
37 H. M. F. Freundlich, *J. Phys. Chem.*, 1906, **57**, 385–471.
38 R. J. Alessio, X. Li and D. F. Martin, *J. Environ. Sci. Health A Tox. Hazard Subst. Environ. Eng.*, 2012, **47**, 2198–2204.
39 Y. Niibori, M. Kunita, O. Tochiyama and T. Chida, *J. Nucl. Sci. Technol.*, 2000, **37**, 349–357.
40 A. A. Inyinbor, F. A. Adekola and G. A. Olatunji, *Water Resour. Ind.*, 2016, **15**, 14–27.
41 R. Ullah, I. Ahmad and Y. Zheng, *J. Spectrosc.*, 2016, **2016**, 1–5.
42 H. Guan, E. Bestland, C. Zhu, H. Zhu, D. Albertsdottir, J. Hutson, C. T. Simmons, M. Ginic-Markovic, X. Tao and A. V. Ellis, *J. Hazard. Mater.*, 2010, **183**, 616–621.
43 H. Zhou, Y. Xu, H. Tong, Y. Liu, F. Han, X. Yan and S. Liu, *J. Appl. Polym. Sci.*, 2013, **128**, 3846–3852.
44 Y.-H. Kim, B. Lee, K.-H. Choo and S.-J. Choi, *Micropor. Mesopor. Mat.*, 2011, **138**, 184–190.
45 R.-Z. Wang, D.-L. Huang, Y.-G. Liu, Z.-W. Peng, G.-M. Zeng, C. Lai, P. Xu, C. Huang, C. Zhang and X.-M. Gong, *RSC Adv*, 2016, **6**, 106201–106210.
46 T. Asada, K. Oikawa, K. Kawata, S. Ishihara, T. Iyobe and A. Yamada, *J. Health Sci.*, 2004, **50**, 588–593.

